SOLUTION MINING RESEARCH INSTITUTE
105 Apple Valley Circle
Clarks Summit, PA 18411, USA

Telephone: +1 570-585-8092
Fax: +1 505-585-8091
www.solutionmining.org

Technical Conference Paper

Mechanical Stability of a Cavern Submitted to High-Frequency Cycles

Benoît Brouard, Brouard Consulting, Paris, France

Attilio Frangi, Politecnico di Milano, Milano, Italy

Pierre Bérest, LMS, Ecole Polytechnique, Palaiseau

SMRI Spring 2011 Technical Conference
18 – 19 April 2011
Galveston, Texas, USA

Solution Mining Research Institute Spring 2011 Technical Conference

MECHANICAL STABILITY OF A CAVERN SUBMITTED TO HIGH-FREQUENCY CYCLES

Benoit Brouard, Brouard Consulting, Paris, France
Pierre Bérest, LMS, Ecole Polytechnique, Palaiseau, France
Attilio Frangi, Politecnico di Milano, Milano, Italy

Abstract

Summary

Storage of natural gas in salt caverns had been developed mainly for seasonal storage, resulting in a small number of yearly pressure cycles and moderate gas-production rates. The needs of energy traders are changing toward more aggressive operational modes. Gas temperature changes and additional stresses generated by high-frequency cycling in a storage cavern are discussed. It is proved that, when short-period gas pressure cycles are performed, the thickness of the thermally disturbed zone at the cavern wall is relatively small. Refined meshes of the disturbed zone are required when performing numerical computations. The case of an actual cavern is discussed. In addition to the Munson-Dawson constitutive law, "reverse" creep is considered. The no-tension and dilation criteria are used to discuss numerical results. It is proved that tensile stresses may develop when cavern pressure is low. The evolution of the state of stresses in the $\left(-I_1/3, \sqrt{3J_2}\right)$ plane; i.e., the "bumble-bee flight", as suggested by Kurt Staudtmeister and Zapf (2010) [1] is discussed, and it is proved that the dilation criterion is met at an early stage.

Key words: Cycling loading, gas cavern design, rock mechanics, numerical analysis

Introduction

Recent changes in the gas market tends to make natural-gas storage caverns operated with much more frequent cycling compared to that in seasonal storage. This implies faster flow rates and shorter recovery periods. This operation mode has also been considered for Compressed Air Storage (CAES) facilities. Cavern stability must be assessed when high-frequency cycles are considered. This paper describes some specific thermo-mechanical issues related to fast pressure and temperature changes.

1. Remarks on time and spatial scales — Meshing

1.1 Pressure/Temperature cycling

In this paper, we discuss the case of a gas-storage cavern. Cavern gas pressure is assumed to take a sinusoidal form:

$$P(t) = \overline{P} + \Delta P \sin(\omega t) \qquad \omega = 2\pi/\tau \tag{1}$$

where $\overline{P}$ is the average gas pressure, ΔP is the amplitude of the pressure cycle, ω is the pulsation, and τ is the cycle period.

Gas warms when its pressure increases and cools when its pressure decreases. In this section we assume that the cycle period is short (Heat flux from the rock mass is neglected.), and the cavern temperature is also sinusoidal:

$$T(t) = \overline{T} + \left(\frac{\gamma - 1}{\gamma}\right)\left(\frac{\overline{T}}{\overline{P}}\right)\Delta P \sin(\omega t) = \overline{T} + \Delta T \sin(\omega t) \tag{2}$$

where $\overline{T}$ is the cavern average temperature, ΔT is the amplitude of the temperature cycle, and $\gamma = C_p / C_v$ is the gas adiabatic index.

Lestringant et al. (2010) [2] give the evolution of salt temperature as a function of radius, r, and time, t, in the case of an idealized spherical cavern:

$$T_{salt}(r,t) = \overline{T} + \Delta T_{salt}(r,t) = \overline{T} + \left(\frac{a}{r}\right)\Delta T \exp\left[-(r-a)\sqrt{\omega / 2k_{salt}}\right]\sin\left[\omega t - (r-a)\sqrt{\omega / 2k_{salt}}\right] \tag{3}$$

where a is cavern radius, and k_{salt} is the salt thermal diffusivity. ($k_{salt} = 3\times10^{-6}$ m^2/s is typical.)

Example #1 — Idealized spherical cavern

Let's consider a small spherical cavern of volume $V \approx 4200$ m^3, with radius $a = 10$ m and average temperature $\overline{T} = 10$ °C, that is submitted to daily sinusoidal pressure and temperature variations, $\Delta T = 10$ °C. The vertical geothermal gradient is taken equal to zero. Figure 1 shows the temperature radial distribution around the cavern wall when the cavern pressure and temperature are maximal. Lestringant et al.'s closed-form solution is compared to finite-element computations performed using LOCAS software (Brouard et al., 2006 [3]). It appears that the steady-state distribution corresponding to the closed-form solution is reached after a few cycles and that the thickness of the thermally disturbed zone is approximately 1.5 m.

Example #2 — Cylindrical cavern

Let's consider a much larger cylindrical cavern of volume $V \approx 500{,}000$ m^3, radius $a = 40$ m and height $H = 100$ m, that is submitted to daily sinusoidal pressure and temperature variations, $\Delta T = \overline{T} = 10$ °C. A refined mesh composed of approximately 140,000 elements was designed to get a precise picture of the temperature distribution around the cavern wall (Figure 2). The thickness of the disturbed zone, which is not dependent on cavern size, still is approximately 1.5 m (5 ft) for this daily cycle. At minimum cavern temperature, which is reached when gas pressure is minimum, it is interesting to note that temperature distribution is not monotonous in the disturbed zone. There is a temperature peak in the salt that is above average temperature and at a distance of approximately $\Delta r \approx 70$ cm (28'') from cavern wall for this daily cycle.

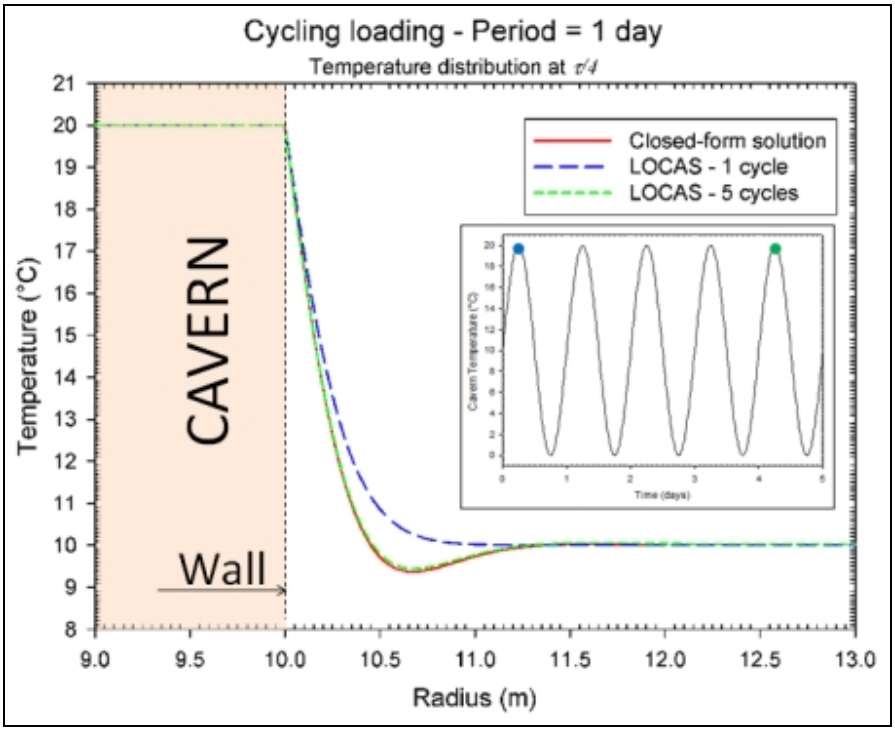

Figure 1 – Example #1 - Small spherical cavern: Radial temperature distribution at the vicinity of the cavern wall. Comparison between a finite-elements code and a closed-form solution.

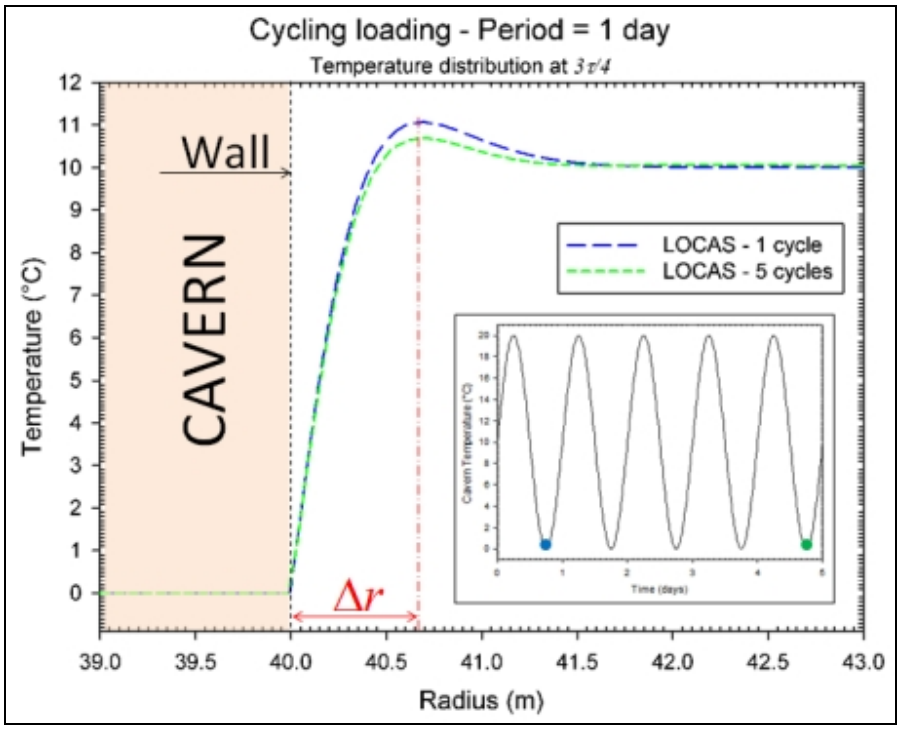

Figure 2 – Example #2 - Large cylindrical cavern: Radial temperature distribution at the vicinity of the cavern wall.

Example #3 — Non-sinusoidal cycling:

Figure 3 shows radial temperature distribution when cavern pressure is minimal in the case of non-sinusoidal loading with a cycling period of one day. The temperature distribution is similar to that in the case of a sinusoidal cycle; in particular, the thickness of the thermally disturbed zone is $\Delta r \approx 70$ cm (28").

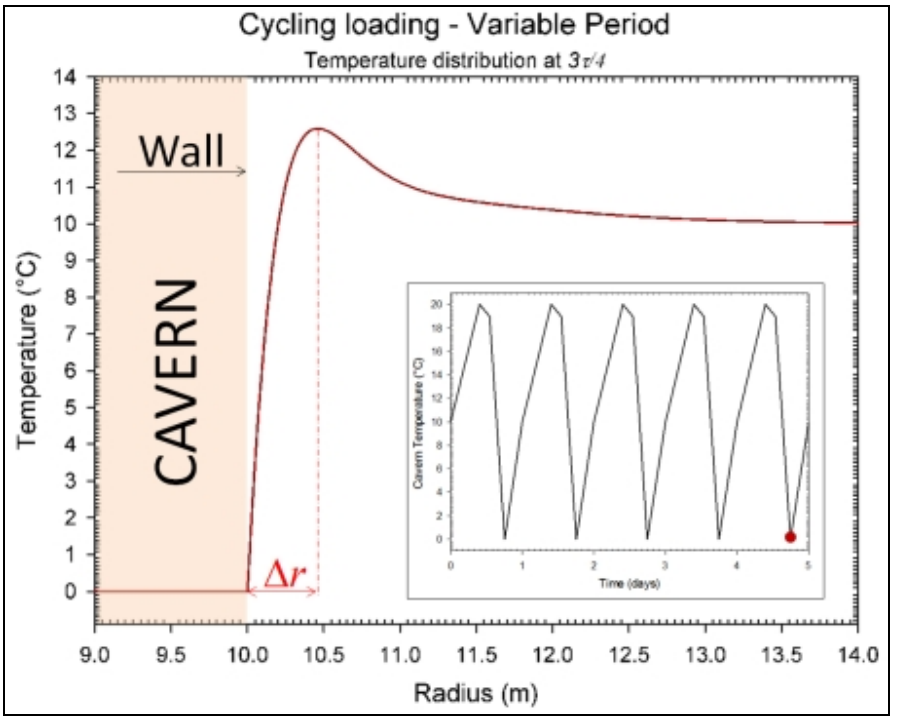

Figure 3 – Example #3 - Small spherical cavern: Radial temperature distribution at the vicinity of the cavern wall, non-sinusoidal cycling.

Example #4 — Effect of cycling period

The effect of the cycling period on temperature distribution in the rock mass is illustrated in Figure 4. The small spherical cavern considered in Example #1 was considered. Cavern temperature was cycled over three different periods: one day, one week end one month. The radial temperature distribution is plotted after 5 cycles when the cavern temperature, and cavern pressure, is the lowest. As can be inferred from closed-form solution (3), the size of the disturbed zone increases with cycle period, or τ. Furthermore, even when the period is relatively large, a temperature peak still can be observed. The thickness, Δr, of the disturbed zone from the cavern wall to peak as a function of sinusoidal cycling periods is shown on Figure 4. It can be inferred from formula (3) that, in this case, thickness Δr can be expressed as:

$$\Delta r = 2.9 \times 10^4 \sqrt{\pi k_{salt} \tau / 2} \qquad (4)$$

where Δr is in cm, salt thermal diffusivity, k_{salt}, in m²/s, and cycling period, τ, in days.

From the former computations, it appears that the thermally disturbed zone in the vicinity of a cavern submitted to daily pressure/temperature variations remains thin, even when the cavern is very large. Furthermore, as large thermo-elastic stresses are triggered by temperature/pressure variations (see

below), a very fine mesh of this disturbed zone is mandatory when finite-element or finite-difference computations are performed.

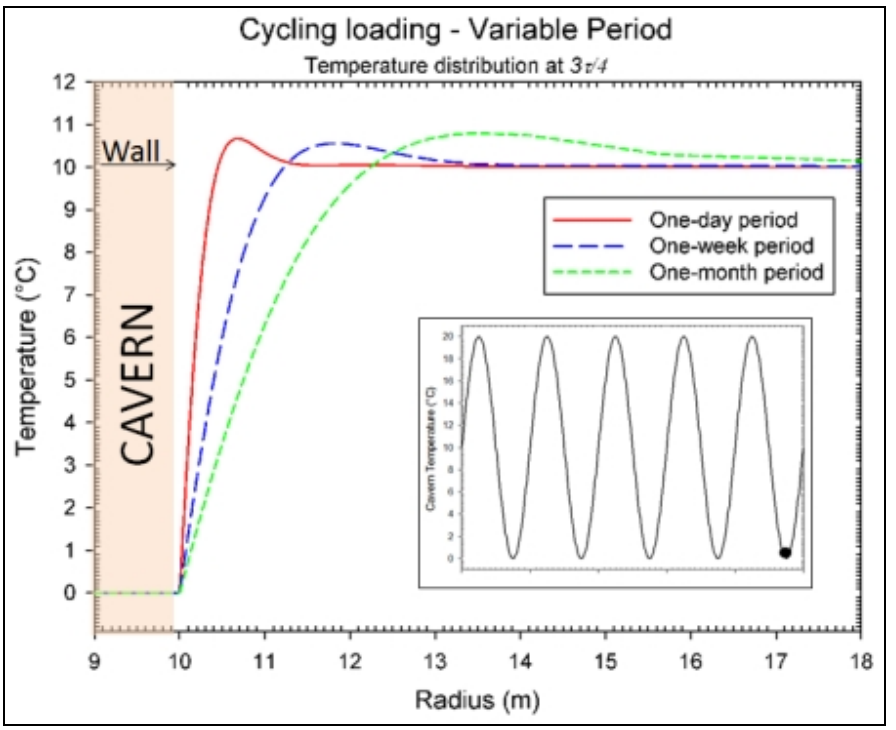

Figure 4 – Example #4 - Small spherical cavern: Radial temperature distribution at the vicinity of the cavern wall, effect of cycling period.

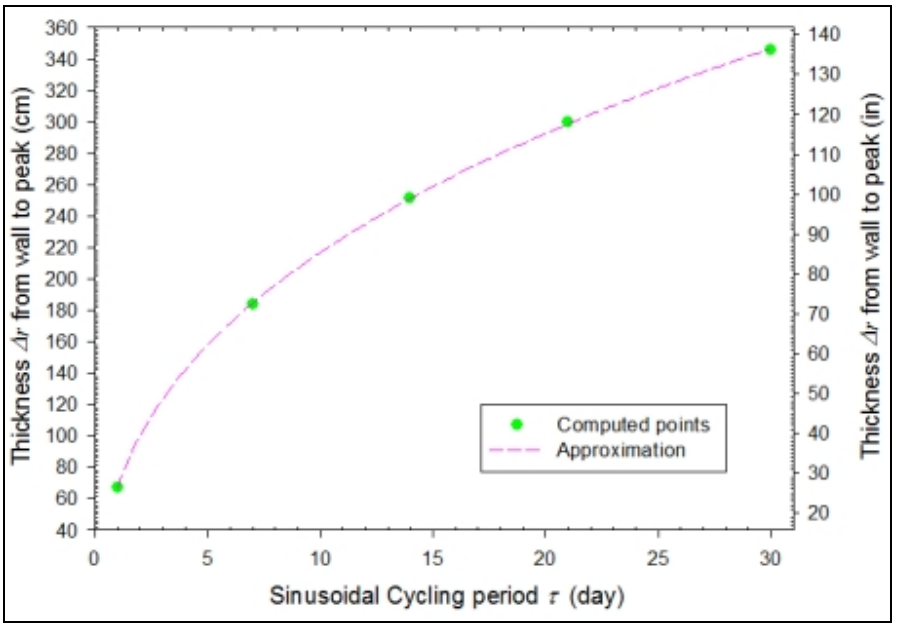

Figure 5 – Thickness, Δr , of the disturbed zone from the cavern wall to peak as a function of sinusoidal cycling period.

1.2 Rules of thumb

When performing numerical computations, including high-frequency cyclic loading, the following spatial and time scales should be considered.

- **Spatial scale** — The thermally disturbed zone must contain at least several elements in the radial direction. A convenient radial size for the largest elements is:

$$\Delta x_{\max} = \Delta r / 5 \tag{5}$$

  Mesh elements should not be radially larger than $\Delta x_{\max}$ inside the annulus between the cavern wall and an outer radius at a distance $2\Delta r$ from the cavern wall.

  For instance, with regard to the daily cycle, $\Delta r \approx 70$ cm, $\Delta x_{\max} = \Delta r/5 \approx 15$ cm $(1/2$ ft$)$, and the outer radius of the disturbed zone is $2\Delta r \approx 1.5$ m (5 ft).

- **Time scale —** Because the size $\Delta x_{\min}$ of the largest element at the cavern wall must be small, the maximum time step, $\Delta t_{\max}$, of the numerical computations should be consistent.

  - ***For 2D computations, the time step*** must be such that

$$\Delta t_{\max} < \Delta x_{\max}{}^2 / 4k_{salt} \tag{6}$$

  - ***For 3D computations, the time step*** must be such that

$$\Delta t_{\max} < \Delta x_{\max}{}^2 / 6k_{salt} \tag{7}$$

  According to formula (4), such a rule holds for sinusoidal thermal loading, but it is relevant still when non-sinusoidal thermal loading, $\Delta t_{\max}$, is considered for 2D computations is a linear function of the cycling period:

$$\Delta t_{\max} < \frac{\Delta r^2}{100 k_{salt}} = \frac{\pi\tau}{200} \tag{8}$$

For instance, the maximum time step ***for 2D daily cycling*** should be $\Delta t_{\max} < \pi/200 \approx 0.02$ day ≈ 23 min.

2. Thermoelasticity

Salt-temperature variations, ΔT_{salt}, induced by cavern-pressure cycling generate additional thermoelastic stresses. These thermoelastic stresses overlap the stress field around the cavern. Closed-form solutions exist when simple shapes are considered. Table 1 gives additional stresses due to temperature variation, $\Delta T_{salt}(r)$, in the salt.

Table 1 – Thermoelastic additional stresses for simple shapes.

Additional stress		Spherical shape	Cylindrical shape
Radial	$\Delta\sigma_{rr}(r)$	$-\frac{2\varpi}{r^3}I(r)$	$-\left(\frac{a}{r}\right)^2 \varpi J(r)$
Tangential	$\Delta\sigma_{\theta\theta}(r)$	$+\frac{\varpi}{r^3}I(r)-\varpi\Delta T_{salt}(r)$	$+\left(\frac{a}{r}\right)\varpi J(r)-\varpi\Delta T_{salt}(r)$
Vertical	$\Delta\sigma_{zz}(r)$	$-\varpi\Delta T_{salt}(r)$	$-\varpi\Delta T_{salt}(r)$

where $\varpi = E_{salt}\alpha_{salt}/(1-\nu_{salt})$, (E_{salt},ν_{salt}) are salt elastic parameters, α_{salt} is the coefficient of thermal expansion of salt, and $I(r)$ and $J(r)$ are integrals defined as follows:

$$I(r)=\int_a^r u^2\Delta T_{salt}(u)\,du \qquad J(r)=\int_a^r u\Delta T_{salt}(u)\,du \tag{9}$$

3. Constitutive law for salt

It is difficult to determine which of the existing constitutive laws for rock salt is the most relevant when considering fast cycling loading. In fact, as suggested by Zander-Schiebenhöfer (2010) [4], it may be necessary to develop new laws based on appropriate laboratory tests.

It is likely that the selected constitutive law should incorporate transient creep and be temperature-dependent. Munson and Dawson (1984) [5] suggested the well-known following model:

$$\dot{\varepsilon}^{ij}=\dot{\varepsilon}_e^{ij}+F\dot{\varepsilon}_{ss}^{ij} \qquad \begin{array}{ll} F=e^{\Delta\left(1-\varsigma/\varepsilon_t^*\right)^2} & \text{when } \varsigma\le\varepsilon_t^* \\ F=e^{-\delta_0\left(1-\varsigma/\varepsilon_t^*\right)^2} & \text{when } \varsigma\ge\varepsilon_t^* \end{array} \tag{10}$$

$$\begin{cases} \dot{\varsigma}=(F-1)\dot{\varepsilon}_{ss} \quad \dot{\varepsilon}_{ss}=A\exp\left(-\dfrac{Q}{RT_{salt}}\right)\left(\sqrt{3J_2}\right)^n \quad \mu=E_{salt}/2(1+\nu_{salt}) \\ \varepsilon_t^*=K_0e^{cT}\sigma^m \quad \Delta = \alpha_w+\beta_w Log_{10}(\sigma/\mu) \qquad \sigma=\sqrt{3J_2} \end{cases} \tag{11}$$

Munson et al. (1996) [6] suggested a modified model that takes into account the onset of “reverse creep” following a stress drop (which is somewhat equivalent to a rapid pressure build-up in a closed cavern). A modified version of this law was proposed by Karimi-Jafari et al. (2005) [7] that allows for simple computations:

$$F=1-\left(1-\varsigma/\varepsilon_t^*\right)^p/(1-k)^p \text{ when } \varsigma>\varepsilon_t^* \tag{12}$$

Reverse creep appears when $\varsigma>k\varepsilon_t^*$, or $F<0$. This modified version of Munson-Dawson model has 11 parameters: $A,n,Q/R,m,\alpha,\beta,K_0,\delta,c,p,k$. Table 2 gives parameters given by Munson (1999) [8] for Avery Island salt.

Table 2 – Munson-Dawson parameters for Avery Island salt.

Parameter	IS UNITS		US UNITS	
	Units	Value	Units	Value
A	/MPa^n-yr	0.74	/psi^n-yr	1.15×10^{-11}
n	—	5.0	—	5.0
Q/R	K	5032	Ra	9058
m	—	3	—	3
α_w	—	-13.2	—	-13.2
β_w	—	-7.738	—	-7.738
K_0	/MPa^m-yr	7×10^{-7}	/psi^m-yr	2.30×10^{-13}
δ	—	0.58	—	0.58
c	/K	0.00902	/Ra	0.00511

Parameters values for reverse creep are $p = 1.1$ and $k = 2.4$ (Karimi-Jafari et al., 2005 [6])

4. Stability — Failure criteria

When dealing with cycling loading and cavern stability, the onset of tensile stresses and salt dilation at the cavern wall must be discussed.

4.1 Tension criterion

When tensile stresses develop at the cavern wall, there is a risk of salt fracturing and spalling. The following two criteria are considered.

- **No Tension** — This criterion stipulates that no main stress must be tensile:

$$\sigma_{\max} < 0 \tag{13}$$

  where $\sigma_{\max}$ is the least compressive of the three principal stresses.

- **No Tensile Effective Stress at the Cavern Wall** — This criterion stipulates that the effective tangential stress at the cavern wall must be negative:

$$\sigma_{tt} + P < 0 \tag{14}$$

  Where σ_{tt} is the less compressive tangential stress. This criterion is much more demanding than the "No-tension" criterion. It is not met when a gas-filled cavern is submitted to a fast and large pressure increase. It must be noted that the relevance of this criterion has not yet been investigated fully.

4.3 Dilation criterion

When shear stresses are large (compared to the mean stress), salt micro-fracturing and dilation take place. These lead to an increase in permeability and a loss of rock strength. Dilatancy is accompanied by a drastic permeability increase, a drop in wave speed, and an increase in acoustic emission. Two dilation criteria are noted here.

- Spiers et al. (1988) [9] proposed a dilation criterion that uses the first invariant of the stress tensor, I_1, and the second invariant of the deviatoric stress tensor, J_2. This well-known dilatancy criterion is written (I_1 and J_2 in MPa):

$$\text{No dilation occurs when} \quad \sqrt{J_2} < -0.27 I_1 + 1.9 \tag{15}$$

- DeVries. (2006) [10] proposed a criterion that distinguishes between a "compressive" state of stresses (typically, $\sigma_3 < \sigma_2 = \sigma_1 < 0$) and an "extensive" state of stress (typically, $\sigma_2 = \sigma_1 < \sigma_3 < 0$):

$$\sqrt{J_2} < \frac{D_1(|I_1|/\sigma_0)^m + \bar{T}_0}{\sqrt{3}\cos\psi - D_2 \sin\psi} \tag{16}$$

Where I_1 and J_2 are in MPa, D_1, D_2, σ_0, $\bar{T}_0$ and m are five empirical constants, $J_3 = s_{ij}s_{jk}s_{ki}/3$ is the third invariant of the deviatoric stress tensor, and ψ is the lode angle such that $\sin 3\psi = -3\sqrt{3}J_3/2J_2^{3/2}$. For the following computations, Cayuta salt parameters were selected (see Table 2).

Table 2 - Selected parameters for DeVries et al. (2006 [10]) dilation criterion.

Parameter	D_1	D_2	n	T_0
Value IS units	0.773 MPa	0.524	0.693	1.95 MPa
Value US units	112 psi	0.524	0.693	283 psi

5. Gas cavern thermodynamics

5.1 Real-gas equation-of-state

The real-gas equation-of-state is used to determine the relationship between temperature, pressure, and density of the considered gas. This equation is defined as:

$$PV = Z\frac{m}{M}RT \tag{17}$$

where m is the gas mass, M is the gas molecular weight, R is the universal gas constant, and $Z = Z(P,T)$ is the gas compressibility factor. For a perfect gas, $Z = 1$, but it may be significantly different for a real gas. For instance, the compressibility factor of Amarillo natural gas is plotted on Figure 6 as a function of pressure and temperature.

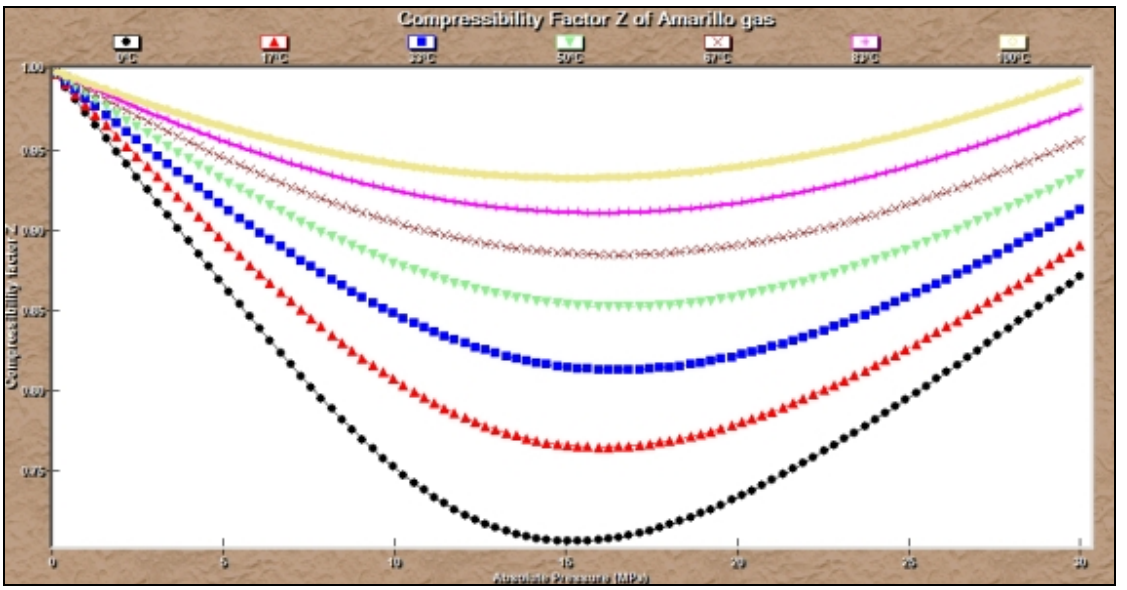

Figure 6 – Compressibility factor of a natural gas a function of pressure and temperature [after SMRI Toolbox].

For coupled computations, it may be useful to approximate the compressibility factor of natural gases using a quadratic equation:

$$Z(P,T) \approx 1 - \left(Z_1 - Z_2 T - Z_3 T^2\right)\left(Z_4 P - Z_5 P^2\right) \tag{18}$$

where Z_i are five gas-specific constants.

5.2 Energy balance

ATG (1986) [11] gives a differential equation inferred from the energy balance of the gas cavern. This equation allows for computation of a gas-temperature rate.

- **During an injection phase**, the formula used in SCTS software can write:

$$\frac{dT}{dt} = \frac{1}{\rho C_v}\left[\frac{T}{\rho}\left(\frac{\partial P}{\partial T}\right)_\rho \frac{d\rho}{dt} + \frac{q_c}{V} + \frac{q_m}{V} C_p \left(T_e - T\right)\right] \qquad \text{[Injection phase]} \tag{19}$$

where P, T, V, ρ are the bulk gas pressure, temperature, volume and density of the cavern, respectively; C_p, C_v are the gas specific-heat capacities, q_c is the heat flux from the rock mass at the cavern wall, T_e is the temperature of gas entering the cavern, and q_m is the mass flow rate of injected gas:

$$q_m = \dot{m} = m\left[\frac{\dot{P}}{P} - \frac{\dot{T}}{T} + \frac{\dot{V}}{V} - \frac{\dot{Z}}{Z}\right] \tag{20}$$

$\dot{V}/V$ is cavern relative volume rate, or

$$\dot{V}/V = \beta_c \dot{P} + \dot{\varepsilon}^{vp} \tag{21}$$

where β_c is the coefficient of compressibility of the cavern, which depends on cavern shape and rock elastic parameters; $\dot{\varepsilon}^{vp}$ is cavern creep rate, which depends on loading history, temperature, cavern shape and salt creep parameters.

- When a **withdrawal phase** is considered, the last term of equation (19) disappears, as it represents the change in gas cavern energy due to the gas flow entering the cavern, a term which vanishes during gas withdrawal because the temperature of the gas flowing out from the cavern is assumed to be equal to the cavern bulk temperature:

$$\frac{dT}{dt} = \frac{1}{\rho C_v}\left[\frac{T}{\rho}\left(\frac{\partial P}{\partial T}\right)_{\rho}\frac{d\rho}{dt} + \frac{q_c}{V}\right] \qquad \text{[Withdrawal phase]} \tag{22}$$

The heat flux from rock mass, q_c, is small compared to the energy change related to the compression/expansion of the gas which is the first term on the right hand side of equation (19). However, the heat flux by conduction from the rock mass may play a significant role when cavern long-term stability is considered. This heat flux can be expressed as follows:

$$q_c = \int_{\partial\Omega} -K_{salt}\frac{\partial T_{salt}}{\partial n}\,da \tag{23}$$

where $K_{salt} \approx 6$ W/m-K is the salt thermal conductivity.

When considering gas cavern thermodynamics in SCTS, heat is assumed to be transferred by convection at the cavern wall. The heat flux then is described using a convective heat-transfer coefficient h:

$$q_c = -k_{salt}\left.\frac{\partial T}{\partial r}\right|_{r=a} = h\left(T_w - T\right) \text{ where } h = 0.1\left[\frac{\alpha g \rho^2 \left(T_w - T\right) C_p {k_{salt}}^2}{\mu}\right]^{1/3} \tag{24}$$

where T_w is the cavern-wall temperature, α is the coefficient of volume expansion of the gas, and μ is the gas dynamic viscosity. This formula is based on the assumption of free convection at a vertical cylinder wall.

In LOCAS, the heat flux, q_c, is calculated directly from the temperature field [equation (23)] taking into account the actual shape of the cavern.

6. Example — Natural-Gas-Storage Loading Scenario

6.1 Cavern shape

Figure 7 shows the shape and mesh of the considered cavern. Its volume is approximately 350,000 m^3 (2.2 MMbbls), the casing-shoe depth is 585 m (1920 ft), the overall cavern height is 83 m (272 ft), and cavern maximum radius is 50 m (164 ft). A chimney develops between the casing shoe and cavern roof, which is 600-m deep (1968 ft).

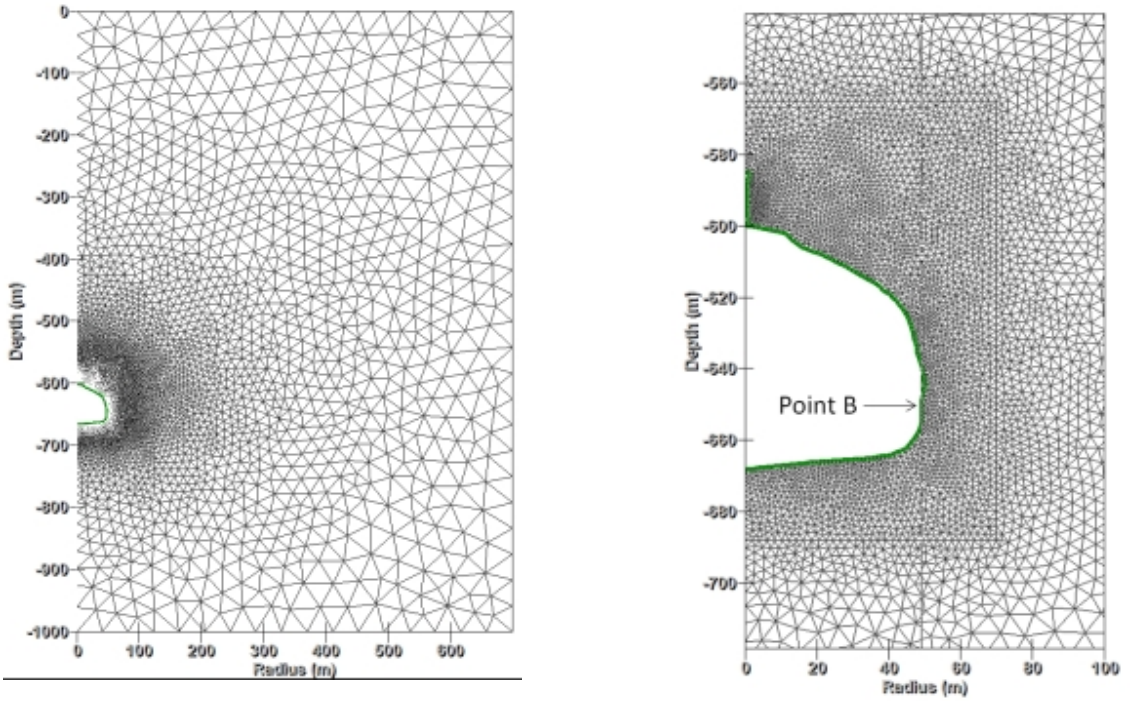

Figure 7 – Natural Gas Storage scenario, Cavern mesh.

6.2 Pressure/Temperature loading

A 400-day leaching period is considered, during which cavern pressure is decreased from geostatic pressure to halmostatic pressure, and brine temperature is decreased from geothermal temperature at an average cavern depth (24°C or 75°F) to 15°C (29°F) at the end of the leaching phase.

When leaching has been completed, the cavern is filled with Amarillo natural gas (Figure 5) and submitted to a pressure-cycle period of $\tau = 2$ days. Pressure amplitude is ΔP = ± 4 MPa (± 580 psi), and the average gas pressure ($\overline{P}$) is halmostatic.

6.3 Cavern temperature

Figure 8 shows the evolution of cavern gas temperature. Temperature variations are large because of large pressure variations. Low temperatures are observed at minimum pressure, because the cavern is relatively shallow and the heat flux from the rock salt is small. When cycling, the average gas temperature slightly increases and tends to a value close to the temperature of the gas injected into the cavern ($T_e = 40$°C in this case).

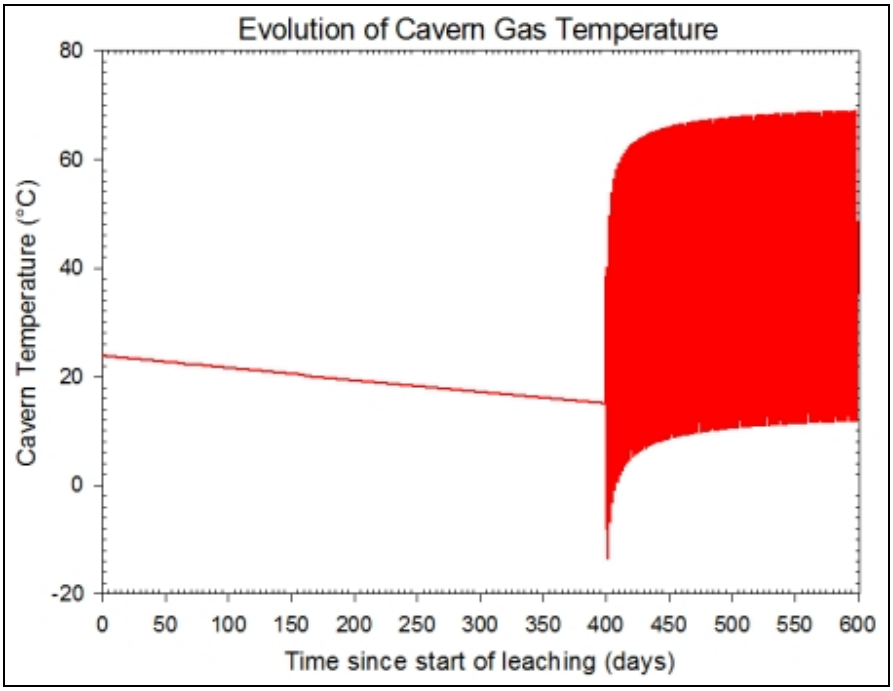

Figure 8 – Evolution of cavern gas temperature.

6.3 Cavern stability

Figure 9 shows tangential stress evolutions at point A located at the bottom of the cavern chimney (Figure 10). The tangential stress becomes tensile when cavern pressure and gas temperature are low during the first cycles but becomes compressive after a few cycles.

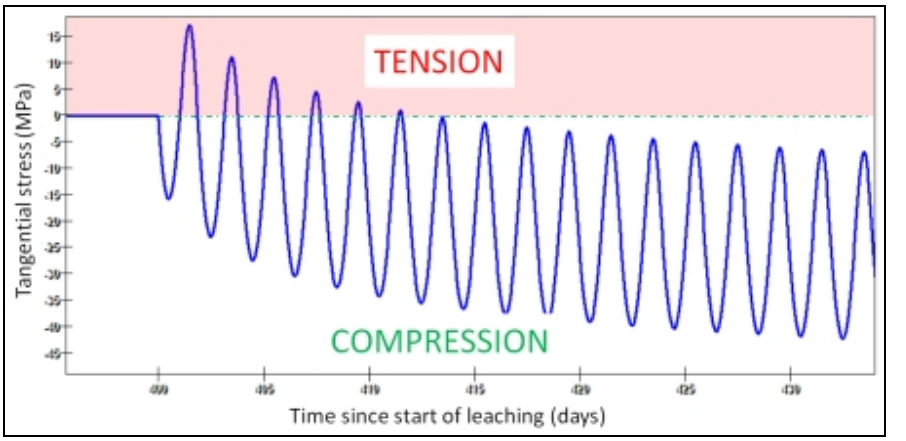

Figure 9 – Evolution of the hoop stress at cavern roof during cycling.

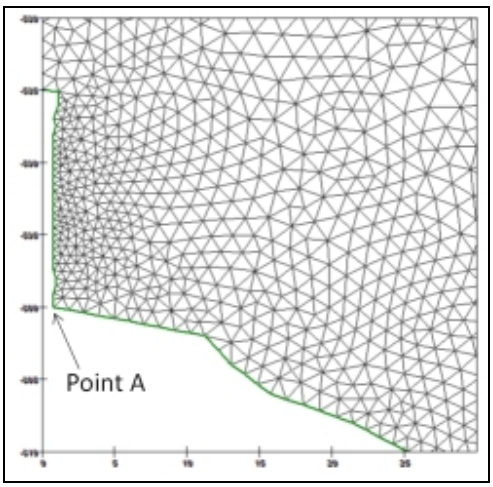

Figure 10 – Cavern roof.

Figure 11 shows a contour plot of the less compressive principal stress in the vicinity of the cavern chimney and roof after 100 cycles, when gas pressure is at its minimum. Only local tensile stresses can be observed on the chimney wall.

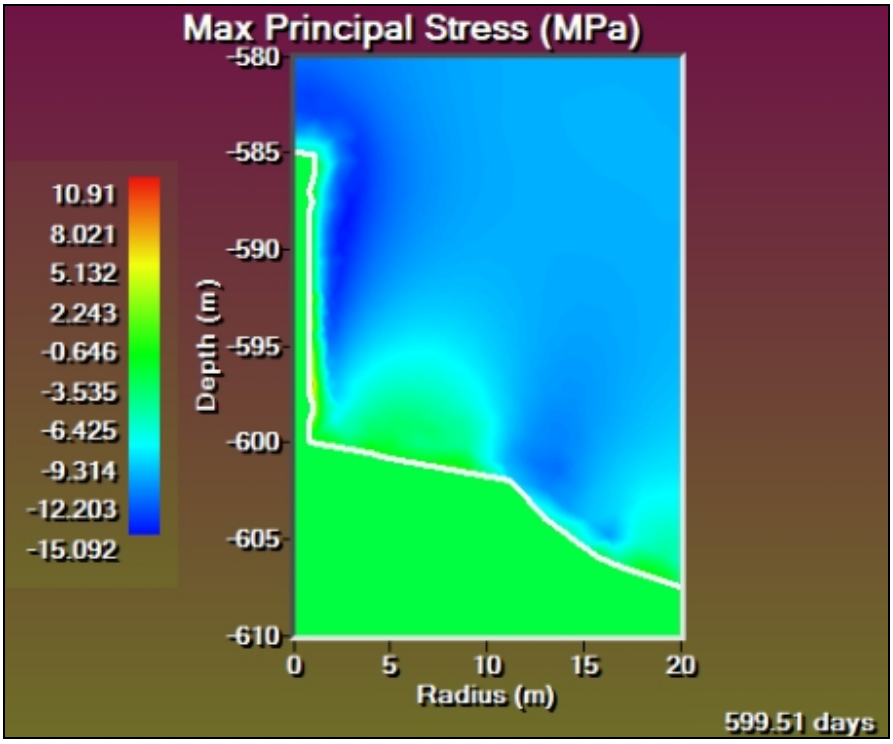

Figure 11 – Cavern roof.

Figure 12 and Figure 13 shows the area of evolution of the state of stress in the $\left(-I_1/3, \sqrt{3J_2}\right)$ plane at point A (cavern roof) and point B (cavern wall). The “bumble-bee flight”, as suggested by Staudtmeister and Zapf (2010) [1], can be observed. When cavern pressure is low, some dilation appears.

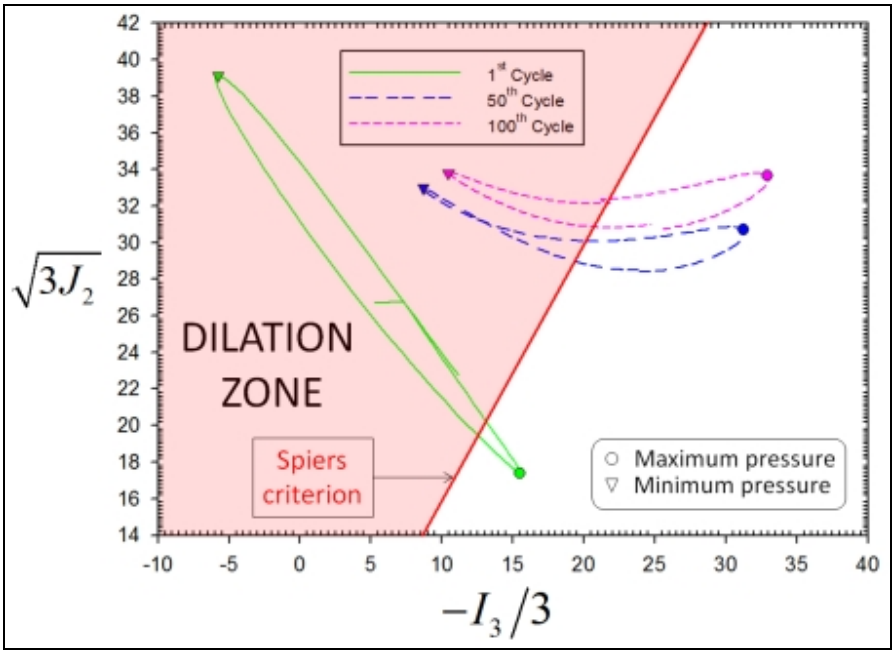

Figure 12 – State of stress at cavern roof (point A) during cycling.

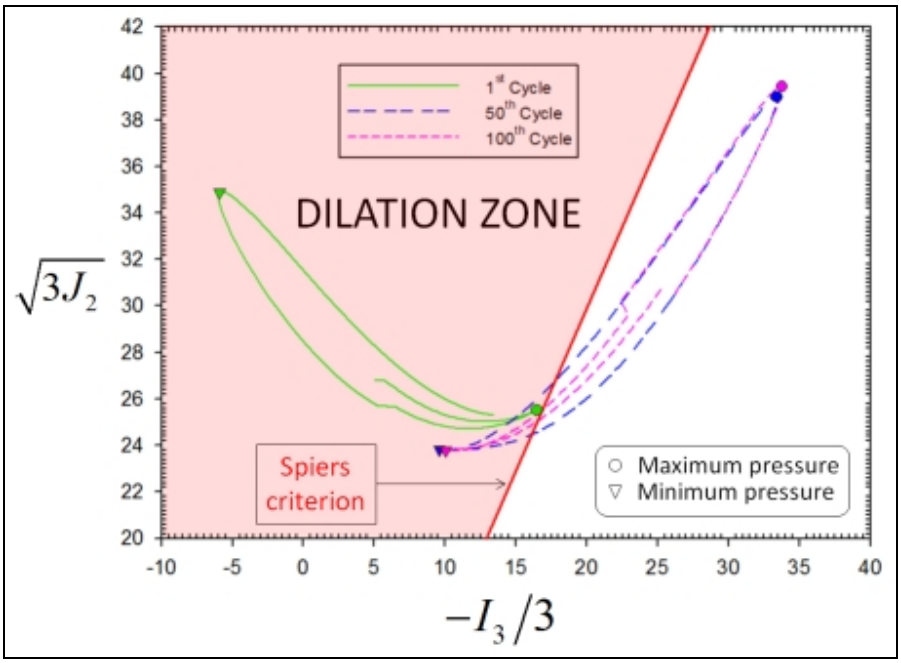

Figure 13 – State of stress at cavern wall (point B) during cycling.

Figure 14 shows a dilation contour plot in the vicinity of the cavern after 100 cycles, when gas pressure is at its minimum. The DeVries criterion has been used. Significant dilatant zone can be observed at the cavern roof.

Figure 15 is a close-up of the former contour plot in the vicinity of the cavern chimney.

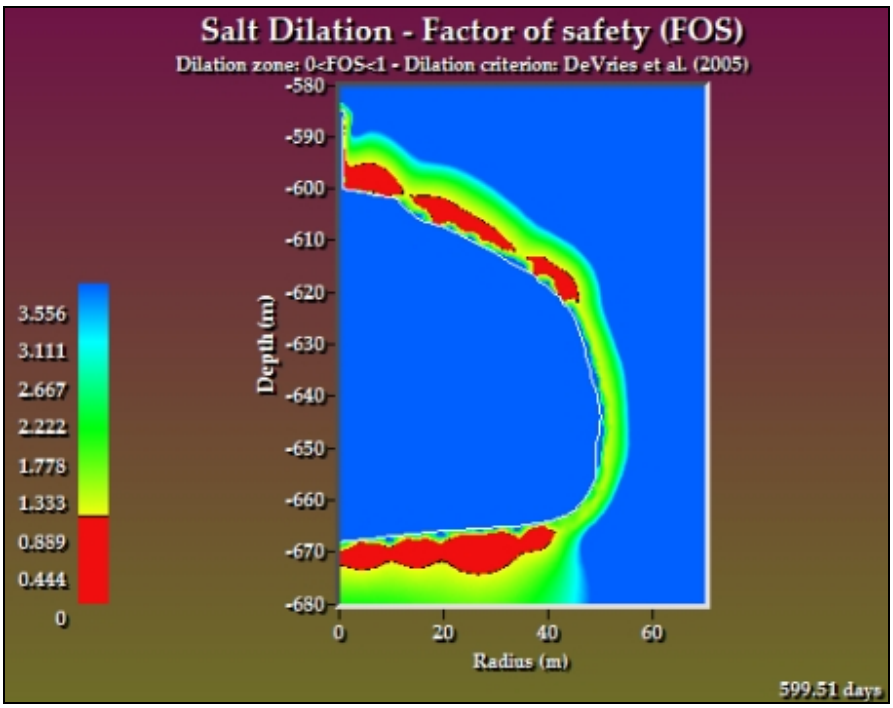

Figure 14 – Dilation criterion in the vicinity of cavern at minimum pressure after 100 cycles [DeVries dilation criterion].

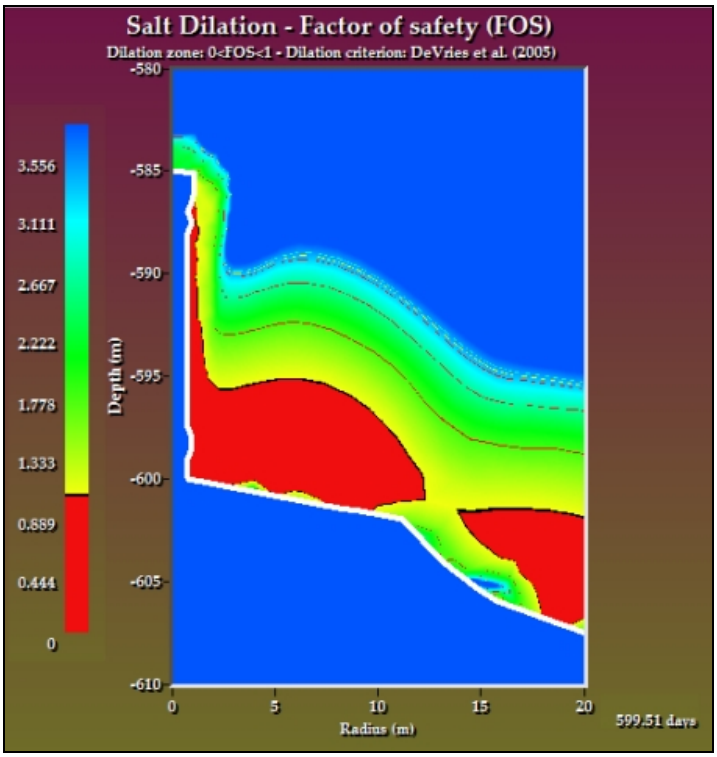

Figure 15 – Dilation criterion in the vicinity of cavern roof at minimum pressure after 100 cycles [DeVries dilation criterion].

7. Conclusions

It was proven that precise computations of temperature variations at cavern wall are possible provided that time steps and elements sizes are correctly selected. Computation of temperature, strains and stresses at the wall and roof of a salt cavern were performed. Munson-Dawson creep law and the same energy balance as used in SCTS were taken into account. It is proved that in the case of a 600-m deep cavern, several zones may experience relative large dilation when the cavern is submitted to high-frequency cycling.

References

[1] ATG *Manuel pour le transport et la distribution du gaz*. Titre XIII – Stockages souterrains de gaz. Association Technique de l'Industrie du Gaz en France (1986).

[2] Bauer S. and Sobolik S. *Pressure cycling in compressed Air and Natural Gas Storage Caverns in Salt: Tracking Stress States and Cavern Closure Using 3-D Finite Element Analysis*. SMRI Spring Meeting, Krakow, Poland, pp.129 (2009).

[3] Brouard B., Karimi-Jafari, M., Bérest P. and Frangi A. *Using LOCAS Software to Better Understand the Behavior of Salt Caverns*. Proc. SMRI Spring Meeting, Brussels, Belgium, pp. 273-288 (2006).

[4] Brouard B., Bérest P. and Karimi-Jafari M. *Onset of tensile effective stresses in gas storage caverns*. Proc. SMRI Fall Meeting, Halifax, Canada, p.119-136 (2007).

[5] DeVries K.L. *Geomechanical Analyses to Determine the Onset of Dilation around Natural Gas Storage Caverns in Bedded Salt*. Proc. SMRI Spring Meeting, Brussels, pp.131-150 (2006).

[6] Karimi-Jafari M., Bérest P., Van Sambeek L., Brouard B. and Bazargan B. *Interpretation of Mechanical Integrity Tests*. Proc. SMRI Fall Meeting, Nancy, France, pp.153-173 (2005).

[7] Lestringant C., Bérest P. and Brouard B. *Thermo-mechanical effects in compressed air storage (CAES)*. Proc. SMRI Fall Meeting, Leipzig, Germany, p.29-44 (2010).

[8] Munson D.E. and Dawson P.R. *Salt constitutive modeling using mechanism maps*. In Proceedings of First Conference on the Mechanical Behavior of Salt. Clausthal-Zellerfeld, Germany: Transactions of Technical Publishers, pp.717-737 (1984).

[9] Munson D.E., DeVries K.L., Fossum A.F. and Callahan G.D. *Extension of the Munson-Dawson model for treating stress drops in salt*. In Proceedings of Third Conference on the Mechanical Behavior of Salt. Clausthal-Zellerfeld, Germany: Transactions of Technical Publishers, pp.31-44 (1996).

[10] Munson D.E. *Correlation of Creep Behavior of Domal salts*. SMRI Spring Meeting, Las Vegas, 3-28 (1999).

[11] Staudtmeister K. and Zapf D. *Rock Mechanical Design of Gas Storage Caverns for Seasonal Storage and Cyclic Operations*. Proc. SMRI Spring Meeting, Grand Junction, Colorado, p.197-214 (2010).

[12] Spiers, C.J., Peach C.J., Brzesowsky R.H., Schutjens P.M., Liezenberg J.L., and Zwart H.J. *Long Term Rheological and Transport Properties of Dry and Wet Salt Rocks*, EUR 11848, prepared for Commission of the European Communities, by University of Utrecht, Utrecht, The Netherlands (1988).

[13] Zander-Schiebenhöfer D. SMRI Research Project – *High Frequency Cycling of Salt Storage Caverns (HFCSSC) – Development of Appropriate Lab Tests & Design Criteria. Step 1: Preliminary Study for a detailed Definition of the Research Needs of the Industry in the Field of HFCSSC* (2010).